Applied Catalysis B: Environmental 185 (2016) 110–118

Contents lists available at ScienceDirect

Applied Catalysis B: Environmental

journal homepage: www.elsevier.com/locate/apcatb

$Pb_{0.04}Co$ catalyst for N_2O decomposition in presence of impurity gases

Haibiao Yu [a], Mamutjan Tursun [b], Xinping Wang [a,*], Xingxing Wu [a]

[a] Key Laboratory of Industrial Ecology and Environmental Engineering (MOE) and State Key Laboratory of Fine Chemical, School of Environmental Science and Technology, Dalian University of Technology, Dalian 116024, China
[b] College of Chemistry and Environmental Science, Kashgar University, Kashgar, Xinjiang 844000, China

ARTICLE INFO

Article history:
Received 3 September 2015
Received in revised form
10 November 2015
Accepted 7 December 2015
Available online 8 December 2015

Keywords:
Dynamics
Pb
Co_3O_4
N_2O decomposition
Resistance to CO_2

ABSTRACT

$Pb_{0.04}Co$(CP) catalyst prepared by coprecipitation method was investigated for N_2O decomposition. It was found that the introduction of Pb into the catalyst greatly decreased the average size of Co_3O_4 crystallites, increased surface area, and active sites in population on the catalyst. The doping of Co_3O_4 with Pb also significantly weakened the Co—O bond, which led to the activation energy decreasing from 74.0 kJ mol^{-1} to 28.9 kJ mol^{-1} and TOF of the reaction at 300 °C increasing from 3.1×10^{-3} s^{-1} to 23.1×10^{-3} s^{-1}. For the reaction over $Pb_{0.04}Co$(CP) in the presence of 5 vol% O_2, 2 vol% H_2O, 500 ppmv NO, 10 vol% CO_2, 50 ppmv SO_2, or some of them, the largest dynamic impact was caused from the NO together with the O_2, which led to a decrease of N_2O conversion from 100% to 40% at 350 °C and 20000 h^{-1}. Whereas, CO_2 had almost no influence on the reaction for the $Pb_{0.04}Co$(CP) catalyst at the reaction conditions.

1. Introduction

Nitrous oxide (N_2O) has been identified as a greenhouse gas and a significant contributor to destruction of ozone in the stratosphere [1–6]. It has been reported that the increasing rate of N_2O in the atmosphere is 0.2–0.3% per year [1,3], and chemical industry in the worldwide is responsible for about 15–25% of them [4]. According to the content of N_2O in tail-gases, the exhaust containing N_2O for the major industrial processes can be divided into the following two kinds: (I) Those with low N_2O concentration (0.05–0.2 vol.%), for instance, the tail-gases caused by the nitric acid production, fossil fuels' combustion, and fluidized-bed combustors. (II) Those with high N_2O concentration (25–40 vol.%), for instance, the tail-gases caused by adipic acid production, and the synthetic processes of acrylonitrile, glyoxal, caprolactam and other chemicals using nitric acid as oxidant/reagent [3–6].

In principle, direct catalytic decomposition of N_2O should be the most convenient and economical method for the abatement of N_2O [7,8], as long as the catalyst is active and stable enough under the reaction conditions. It has been successfully developed to eliminate N_2O from the tail-gases in the kind (II) [4,9–11], due to the temperature increasing caused by the exothermic reaction. However, no application of this method was found yet for the tail-gases in the kind (I), because the temperature increasing is negligible and the catalyst can not work effectively at lower temperature. Especially, in most of the cases, O_2, NO_x, H_2O even CO_2 are present in the tail-gases, which considerably suppress the activity of the catalysts [12] at the lower temperature. In some cases, SO_2 also appears in the tail-gases, such as in the engine exhaust after TWC (three ways catalyst) or NSR (nitrogen oxides storage reduction) treating. Thus, a catalyst active for the N_2O decomposition at the lower temperature and stable in the presence of impurity gases is desired for applying the method to tail-gases in the kind (I).

For the direct catalytic decomposition of N_2O, most researchers studied their catalyst only under ideal reaction conditions (without impurity in the feed gas), or in the presence of O_2, and H_2O [13–19]. They found that O_2 and H_2O in the feed gas largely decreased the activity of the catalysts for the reaction. Russo et al. reported that $MgCo_2O_4$ catalyst was more active than $ZnCo_2O_4$ and $CoCo_2O_4$, over which the T_{50} (the temperature for the N_2O conversion reaching 50%) of the reaction were 440 °C and 470 °C in the absence and presence of 5 vol% O_2, respectively [13]. Asano et al. have reported that K-doped Co_3O_4 catalyst with K/Co ratio of 0.02 was rather active for the reaction in the absence of H_2O, over which the N_2O conversion reached to 80% at 200 °C, whereas it became negligible under the presence of 2.5 vol% H_2O at the reaction temperature [14]. Similar result was also reported by Pasha and the coworkers for the reaction over Cs/Co-0.05 [15], and Cs/Cu-0.1 [16] catalysts. The authors found that the extent of the reaction being inhibited by 4 vol% O_2 significantly depended on the kinds of transitional metal

* Corresponding author.
E-mail address: dllgwxp@dlut.edu.cn (X. Wang).

http://dx.doi.org/10.1016/j.apcatb.2015.12.011
0926-3373/

of the catalyst, while that caused by 2 vol% H_2O was always greater, irrespective of the catalyst composition. As for the mechanism of O_2 and H_2O inhibiting the reaction, they have suggested that it arisen from the two impurity gas molecules competitively adsorbing on active sites with N_2O.

It seems that the inhibition effect of NO and NO_2 on the reaction is more serious for the general catalysts compared to those of O_2 and H_2O [20–33]. Xue et al. investigated the influence of 10 vol% O_2, 3 vol% H_2O, and 500 ppmv NO on the reaction over an optimized $CoCe_{0.05}$ catalyst. They found that the inhibitory effect of the impurity gases on the reaction increased in the order $O_2 < H_2O < NO$ [20]. However, as reported by Zabilskiy et al., the reaction inhibited by 1.5 vol% H_2O over Cu/CeO_2-160 was much more severe than that by 1.5 vol% NO at 500 °C [33]. Kuboňová et al. compared the influence of 5 vol% O_2 and 1.8–2.3 vol% H_2O, and both of them with 200 ppmv NO in the feed gas 1000 ppmv N_2O/N_2 on the reaction over 2.7% Rh/Al-MCM-41. They found that the T_{50} for feed gas 1000 ppmv N_2O/N_2 was 245 °C, while it shifted to 305 and 388 °C in the two latter cases, respectively [21]. As NO_2 could be produced by NO reacting with O_2, the negative influence caused by NO together with O_2 on the reaction may be quite different from that arisen from the NO alone in the feed gas. Rutkowska et al. found that hierarchical Beta zeolite exchanged by Fe^{2+}, or Co^{2+} was more stable in catalytic activity than that exchanged by Cu^{2+} for the feed gas containing 4 vol% O_2, 3 vol% H_2O and 200 ppmv NO in 1000 ppmv N_2O/He [22]. Zhang et al. have reported that indium added into Co-MOR greatly improved the catalytic stability of the catalyst, and due to which, high N_2O conversion (90%) was obtained over CoIn-MOR at 450 °C with time on stream of 100 h for the feed gas composed of 5000 ppmv N_2O, 1000 ppmv NO, 5 vol% O_2, and 2 vol% H_2O in He [23]. Recently, a much active and stable catalyst, $0.01K\text{-}Cu_{0.25}Co_{2.75}O_4$, was reported by Franken et al., over which N_2O conversion higher than 70% was observed when feed gas 1000 ppmv N_2O, 2 vol% O_2, 0.5 vol% H_2O and 200 ppmv NO in N_2 passed though the catalyst bed at 400 °C with 54,000 h^{-1} [24].

Previously, Pérez-Ramírez et al. reported that the reaction over Fe^{3+} exchanged ZSM-5 catalyst (ex-FeZSM-5) was positively influenced by 250 ppmv SO_2 in the feed gas, while the influence of 0.5 vol% CO_2 on the reaction was negligible [12]. Komvokis et al. found that the addition of 50 ppmv SO_2 into the feed gas resulted in a pronounced and irreversible deactivation of the $Ru/\gamma\text{-}Al_2O_3$ catalyst [4]. They suggested that stable sulphate species formation on the catalyst surface was responsible for it. However, there are seldom investigations later being concerned with CO_2 and SO_2, whereas these impurity gases are generally contained in the tail-gases coming from combustion processes. Recently, we found that the activity of $Bi_{0.02}Co$ catalyst was hardly influenced by 10 vol% CO_2, while $K_{0.01}Co$ catalyst due to the CO_2 lost its most activity [34]. In this paper, we report $Pb_{0.04}Co$ catalyst, which is more active than $Bi_{0.02}Co$ in the presence of CO_2, O_2, and H_2O. As the aim of the present work is to explore a possible catalyst, which can combine with TWC or NSR catalyst to eliminate N_2O from the engines' exhaust, the activity of the catalyst for N_2O decomposition influenced by NO, SO_2, together with O_2 was also studied.

2. Experimental

2.1. Catalyst preparation

The Pb_xCo catalysts (x = 0–0.2) were generally prepared by coprecipitation method in the following procedures. 0.5 M Na_2CO_3 aqueous solution was added dropwise to a mixed solution containing desired amounts of $Co(NO_3)_2{\cdot}6H_2O$ and $Pb(NO_3)_2$ at 40 °C under drastic stirring until the pH of the solution approximately reached to 9.3. The slurry was stirred for additional 2 h before it was filtered. Then the resultant precipitate was washed with distilled water until the pH of the filtrate reached to 7. To ensure that the wash process is sufficient so that the residual sodium content in the precipitate does not influence the activity of resulting catalysts, the wash-filtrating was carried out for at least 8 h in a continuous filtrating column. Finally, the precipitate was dried at 110 °C for 4 h, followed by calcination at 500 °C in static air for 3 h. According to the mole ratios of $Pb(NO_3)_2$ to $Co(NO_3)_2{\cdot}6H_2O$ in the mixed solution (x), the catalysts were labeled as Pb_x Co(CP). The two extreme cases, were Co_3O_4(CP) and PbO_x (CP), respectively, which were obtained from $Co(NO_3)_2{\cdot}6H_2O$ or $Pb(NO_3)_2$ alone for precipitation.

For comparison, the $Pb_{0.04}Co$ catalyst was also prepared by impregnation method and citric acid method, which were correspondingly labeled as $Pb_{0.04}$Co(IM) and $Pb_{0.04}$Co(CA), respectively. For preparing the $Pb_{0.04}$Co(IM) catalyst, $Pb(NO_3)_2$ aqueous solution was used to impregnate the Co_3O_4(CP) that was obtained by the coprecipitation method (x = 0); For preparing the $Pb_{0.04}$Co(CA) and pure Co_3O_4(CA) catalyst samples, $Co(NO_3)_2$ alone or together with $Pb(NO_3)_2$ in appropriate amounts was dissolved in distilled water. Then, citric acid monohydrate was added to the mixture in moles twice of (Co + Pb) under continuous stirring. Subsequently, the water was removed at 90 °C until a viscous gel was formed. Finally, the gel was dried overnight at 110 °C, and calcined at 500 °C for 3 h in air.

2.2. Catalyst characterization

XRD patterns were recorded with an X'Pert Pro MPD multipurpose diffractometer (PANalytical, Inc.), which employed Cu Kα radiation (λ = 1.5406 Å) and operated at 40 kV and 30 mA. Diffraction patterns were recorded with scan step of 0.026° at the speed of 22.44 s/step for 2θ from 10 to 80°. Average sizes of the catalyst crystallines were estimated according to Scherrer equation based on the half-height width of the peak 2θ = 36.8° (311).

Transmission electron microscopy (TEM) was used for observing the morphology of the crystallites in the catalysts, for which the powder sample was suspended in ethanol and the suspension was dropped onto copper grids with holey carbon films. The average size of the crystallites in the catalyst was obtained from a statistical calculation based on the data of at least 40 crystallites in the catalyst.

Nitrogen adsorption–desorption isotherms were obtained at −196 °C using an ASAP 2020 volumetric analyzer, for which the samples were degassed at 200 °C under high vacuum for 1 h prior to the measurements. BET model was used to estimate the surface areas of the samples.

CO adsorption IR spectra were recorded on a Bruker TENSOR 27 FTIR Spectrophotometer at a resolution of 4 cm^{-1} for 16 scans (1 s per scan). For the experiment, self-supporting catalyst wafer or KBr-mixed disc with a diameter of 13 mm was pretreated by N_2 at 300 °C in quartz IR cell equipped with CaF_2 windows for 30 min, cooled to 110 °C for taking skeletal spectrum of the catalyst (S_C) under evacuation. Then the sample was exposed to 11.3 vol% CO/N_2 for taking saturated CO adsorption spectrum, in which the corresponding S_C was exactly subtracted.

X-ray photoelectron spectra (XPS) measurements of the catalysts were conducted on a Thermo ESCALAB 250Xi using an AlKa source. The carbonaceous C 1 s binding energy of 284.8 eV was used as a reference for determining the binding energies.

O_2 pulse adsorption and temperature programmed desorption of O_2 (O_2-TPD) was performed on Chem BET Pulsar TPR/TPD. Each sample (0.300 g) was pretreated in situ at 300 °C for 20 min in He flow. Then it was subsequently cooled down to 100 °C, O_2 was injected in pulses (200 μL) until saturated adsorption was reached, and after that it was cooled down to a temperature lower than 50 °C

in He, to start the O_2-TPD in the flow at temperature ramp rate of 10 °C/min.

2.3. Activity tests and dynamic study

Activity of the catalysts for N_2O direct decomposition was tested in an integral fixed bed continuous flow quartz reactor (with an inside diameter of 4 mm). Gas mixture being composed of 2000 ppmv N_2O in Ar or that with some of the impurity gases (5 vol% O_2, 2 vol% H_2O, 500 ppmv NO, 10 vol% CO_2, 50 ppmv SO_2) was fed to 0.200 g (40–60 mesh) catalyst at gas hourly space velocity (GHSV) 20000 h^{-1}. It was confirmed that neither external nor internal mass transport resistance influencing the reaction for the $Pb_{0.04}Co$ catalyst at 300 °C, by feeding the gas flow at 50 ml/min to 0.2 g catalyst and at 75 ml/min to 0.30 g catalyst, as well as changing particle size of the catalyst from 40–60 mesh to 60–80 mesh. Both the inlet (dry feed gas) and effluent gas (after condensation for removing some of H_2O) were analyzed (refer to Fig. S1) by gas chromatography equipped with a porapak Q column (4 m in length and 2.1 mm in inner diameter), using TCD as detector. Steady-state catalytic activity was measured at temperatures between 150 and 450 °C, in step of 50 °C. Based on the N_2O concentrations of incoming ($c(N_2O)_{in}$) and effluent ($c(N_2O)_{out}$), N_2O conversion was calculated according to the equation

$$\text{Conv.}\% = \frac{c(N_2O)_{in} - c(N_2O)_{out}}{c(N_2O)_{in}} \times 100\% \quad (1)$$

To obtain kinetic parameters, the reaction was carried out on a differential quartz reactor (with an inside diameter of 2.2 mm). In this case, 0.0083–0.180 g catalyst (60–80 mesh) was used and the N_2O conversion was controlled in the range of 7–15% to minish systematic analysis error as well as the deviation resulted from reactant concentration change in the catalyst bed.

Specific reaction rate (r), rate constant (k), activation energy (E_a) and turnover frequency (TOF) were respectively calculated according to the following equations:

$$r = \frac{p_0 \times F \times 2000 \times 10^{-6}}{R \times T_0 \times m_{cat}} \times \text{conv.}\% \left(\mu\text{molS}^{-1}\text{g}_{cat}^{-1}\right) \quad (2)$$

$$k = \frac{r}{\bar{c}} \quad (3)$$

$$\text{TOF} = \frac{r}{n} \quad (4)$$

In Eq. (2), p_0 is atmospheric pressure (101325 Pa), F (ml s^{-1}) is the total flow rate of feed gas mixture, R is gas constant (8.314 J K^{-1} Mol^{-1}), m_{cat} (g) is the amount of the catalyst, T_0 is the room temperature (298 K); In the Eq. (3) $\bar{c}$(μmolm^{-3})is the N_2O concentrations averaged from those at the inlet and outlet of the reactor; In the equation (4), n μmol g_{cat}^{-1} is the amount of active sites detected by O_2-TRD. The activation energy was determined based on the reaction data in the temperature ranges 473–573 K for $Pb_{0.04}Co$(CP), 573–673 K for Co_3O_4(CP), according to Arrhenius equation.

For kinetic parameters, in addition to the direct determination in differential reactor, they were also estimated based on our integral reaction results. In the later case, the N_2O concentrations at each definite catalyst bed layer were calculated, according to the reaction order that was confirmed to be the first order by our experiments.

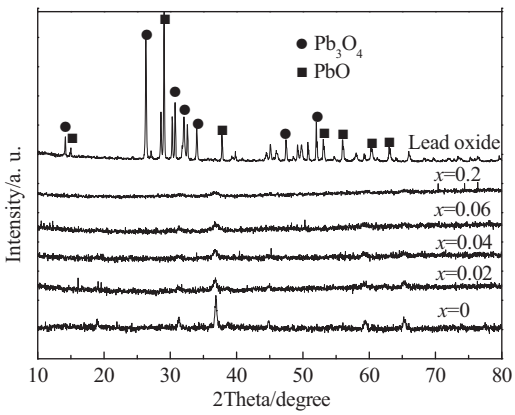

Fig. 1. XRD patterns of the Pb_xCo(CP) catalyst samples.

Table 1
Comparison of the catalysts on their surface area and average crystal size.

Catalysts	BET surface area (m^2/g)	Crystal size (nm)	
Co_3O_4 (CP)	11.7	33[a]	33.8[b]
$Pb_{0.04}Co$ (CP)	64.7	12[a]	11.4[b]

[a] Calculated from XRD.
[b] Observed by TEM.

3. Results and discussion

3.1. Textural structure and surface property of the catalysts

3.1.1. Textural structure and associated possible mechanism

Fig. 1 presents the XRD patterns of the Pb_x Co(CP) catalysts (x = 0–0.2), from which it can be seen that all the diffraction peaks of the catalysts belong to the Co_3O_4 spinel structure (JCPDS 43–1003). For the samples containing Pb, the diffraction peaks were markedly broadened compared with those of pure Co_3O_4(CP), and the extent was increased with the x increasing in the range of 0–0.06. Average sizes of the Co_3O_4 crystallines were estimated for the pure Co_3O_4(CP) and $Pb_{0.04}Co$(CP) catalysts, according to Scherrer equation, which were 33 and 12 nm, respectively (Table 1). The results were in accordance with the BET surface areas of the two samples, 11.7 m^2/g for Co_3O_4(CP) and 64.7 m^2/g for $Pb_{0.04}Co$(CP) (Table 1).

Fig. 2 shows TEM morphologies of the crystallites in Co_3O_4(CP) and $Pb_{0.04}Co$(CP). It can be seen that the crystallites in the former ranged from 25 to 40 nm, with an average size of 33.8 nm, while those in the latter ranged from 9 to 14 nm, with an average size of 11.4 nm (Table 1). The results agree well with those estimated from XRD.

Herein, it should be noticed that neither new phases other than Co_3O_4, nor the peak shifting were observed for the Pb_xCo(CP) catalysts (x = 0–0.06) in XRD. To study the presence state of Pb in the catalysts, a catalyst sample $Pb_{0.2}Co$(CP) with the PbO content of 35.7 wt.% was prepared and analyzed by XRD. Surprisingly, the same phenomena still appeared (Fig. 1). The results mean that the Pb existed neither separately as its oxides nor as a compound combined with Co. The Pb in the Pb_xCo(CP) catalysts should not be present as solid solution with Co as well, as no peak shifting due to the larger radius (120 pm) of Pb^{2+} than that of Co^{2+} (72 pm) could be observed. On the other hand, strong diffraction peaks appeared on the PbO_x(CP) sample that was obtained from $Pb(NO_3)_2$ precipitation. Thus, for $Pb_{0.04}Co$(CP) catalyst, it is reasonable to speculate that Pb most probably presents on the Co_3O_4 crystallites' surface, and hence it was highly dispersed in the catalyst.

The speculation was validated by XPS measurement. As shown in Table 2, the atomic ratio given by the XPS was 0.095, which was about twice of that calculated by the molecular ratio of $Pb(NO_3)_2$

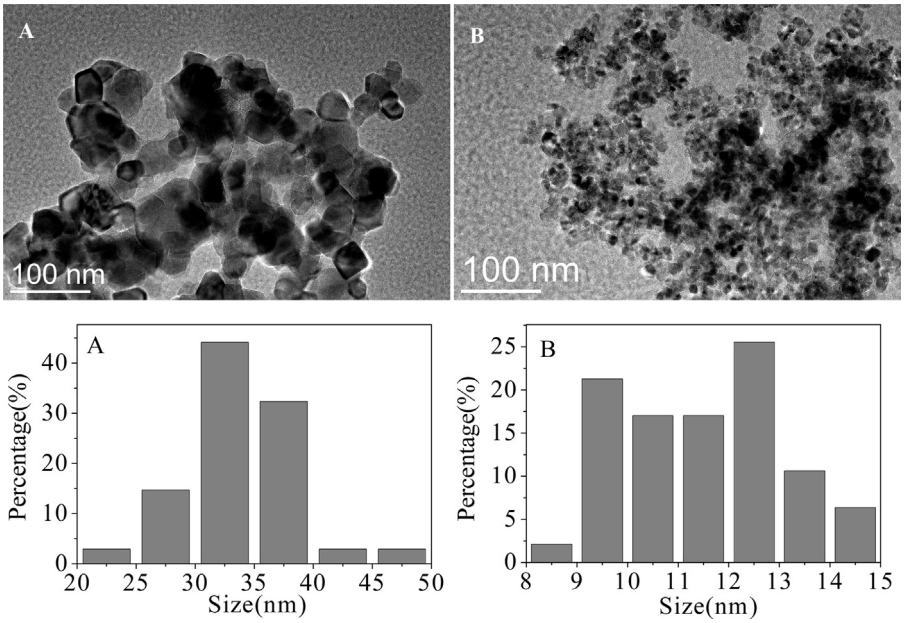

Fig. 2. TEM photos and crystallite size distribution of Co_3O_4(CP) (A) and $Pb_{0.04}Co$(CP) (B) samples.

Table 2
XPS results of $Pb_{0.04}Co$ and Co_3O_4.

Catalysts	Binding energy (eV)				Atomic ratio of Pb/Co
	$Co2p_{1/2}$	$Co2p_{3/2}$	$Pb4f_{5/2}$	$Pb4f_{7/2}$	
Co_3O_4	794.9	779.9	–	–	–
$Pb_{0.04}Co$	794.8	779.9	143.0	138.1	0.095

to $Co(NO_3)_2{\cdot}6H_2O$ used for coprecipitation. Taking account of that the depth generally measured by the XPS is 3–5 nm, it can be considered that the actual atomic ratio of Pb to Co on the $Pb_{0.04}Co$(CP) catalyst surface should be much larger than the datum given by the XPS measurement. Therefore, it can be concluded that the Pb in $Pb_{0.04}Co$(CP) catalyst predominantly exists on the Co_3O_4 crystallites' surface.

Thus, the possible mechanism for the presence state of Pb can be tentatively described as follows: As the concentration of Co^{2+} was absolutely larger compared with that of Pb^{2+} in the solution for coprecipitation and that the solubility product constants (7.4×10^{-14} for $PbCO_3$ and 1.4×10^{-13} for $CoCO_3$) are much closed to each other, the $CoCO_3$ crystallites must be firstly produced in the coprecipitation. During this procedure, the Pb^{2+} cation may hardly incorporate into the $CoCO_3$ crystal lattice, due to its much larger radius compared with that of Co^{2+} cation. Thus, once a Pb^{2+} cation bonded to CO_3^{2-} anion on the crystallite surface, it would interrupt the further growth where for the crystallite. As the results, the average crystalline size of Co_3O_4 in $Pb_{0.04}Co$(CP) catalyst must be considerably less than that in pure Co_3O_4(CP) sample, as measured by XRD and TEM, and therefore Pb in the $Pb_{0.04}Co$(CP) catalyst must predominantly exist on the catalyst surface, as measured by XPS analyses.

To verify the mechanism, the $Pb_{0.04}Co$(CA) sample was measured by XRD (Fig. S2). Interestingly, the sample displayed its clear PbO phase together with that of Co_3O_4, though it has the same Pb content with that of $Pb_{0.04}Co$(CP). Furthermore, from the half-height width of the peak, it can be deduced that the average size of Co_3O_4 crystallites in the $Pb_{0.04}Co$(CA) (22 nm) was much larger than those in $Pb_{0.04}Co$(CP) (12 nm). These results indicate that the average size decreasing of the Co_3O_4 crystallites due to the Pb presence in the catalysts is significantly associated with catalyst preparation method, which strongly supports the mechanism mentioned above. Herein, it should be noted that the average size of Co_3O_4 crystallites in the $Pb_{0.04}Co$(CA) (22 nm) was also obviously less than that (41 nm) in the Co_3O_4(CA) sample (not shown). The little Co_3O_4 crystallites should be resulted from possible splitting of some lager Co_3O_4 crystallites during calcination, where some Pb^{2+} cations were incorporated in, due to the much larger radius of Pb^{2+} than that of Co^{2+}.

3.1.2. Surface property

It has been proposed that the K^+ cations cause the electron donation from the oxygen anions to the cobalt cations and therefore weaken the Co—O bond [35,36]. To investigate the surface property of Co_3O_4 influenced by Pb, CO adsorption IR spectra on Co_3O_4(CP) and $Pb_{0.04}Co$(CP) were recorded (Fig. S3A). On Co_3O_4(CP), the band due to CO adsorption on Co^{2+} appeared at 1646 cm^{-1}, while it shifted to 1635 cm^{-1} on $Pb_{0.04}Co$(CP). To confirm that the band is characteristic for CO adsorbed on Co^{2+} cations and that the wavenumber of the band is associated with electric property of the Co cations, the CO adsorption IR spectra on a $K_{0.01}Co$(IM) self-supporting wafer and on a disc prepared by grinding Co_3O_4(CP) with KBr were recorded (Fig. S3B). On the $K_{0.01}Co$(IM) sample, as expected, the band shifted to 1616 cm^{-1}. Even on the sample of Co_3O_4(CP) ground with KBr, the band shifting from 1646 cm^{-1} to 1627 cm^{-1} could be observed. Fig. 3 compares the CO adsorption spectra on Co_3O_4(CP), $Pb_{0.04}Co$(CP) and $K_{0.01}Co$(IM). It can be found that the band on $Pb_{0.04}Co$(CP) was at 1635 cm^{-1}, which is lager than that of $K_{0.01}Co$(IM) (1616 cm^{-1}) while less than that of Co_3O_4(CP) (1646 cm^{-1}) in wave number. These results indicate that Pb^{2+} in the $Pb_{0.04}Co$(CP) catalyst has the electron donation effect similar to that of K^+, though the effect is not comparable with the latter.

In literature, the Co $2p_{3/2}$ was usually applied to characterize the strength of Co—O bond [14,37–39], whereas, no large difference in the binding energy (BE) indicating the function of Pb^{2+} weakening the Co—O bond can be recognized by the XPS measurements on Co_3O_4(CP) and $Pb_{0.04}Co$(CP). As shown in Table 2, the two samples exhibited the same BE of 779.9 eV for Co $2p_{3/2}$, though their Co $2p_{1/2}$ (794.9 and 794.8 eV) was slightly different. It may arise from the following two reasons: (1) XPS detects the atoms at least 3 nm deep below the catalyst surface, whereas Pb in the $Pb_{0.04}Co$(CP) pre-

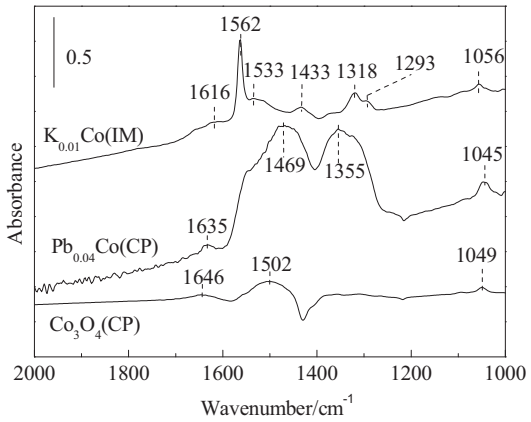

Fig. 3. Steady FTIR absorption spectra of CO on $K_{0.01}$Co(IM), $Pb_{0.04}$Co(CP) and Co_3O_4(CP) at room temperature.

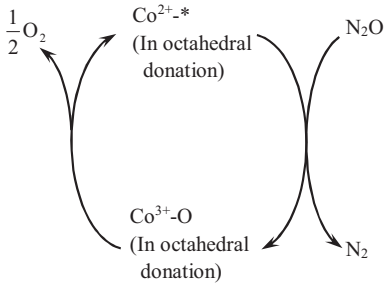

Fig. 4. Chemical state change for the active sites in the catalytic cycles.
Note: Co^{2+}-* stands for the oxygen vacancy associated with the active site.

dominantly presents at the catalyst surface, as mentioned above; (2) Pb weakening the Co—O bond is not comparable with alkali and alkaline earth metals in the extent.

Table 2 also represented the binding energy of Pb $4f_{5/2}$ (142.98 eV) and Pb $4f_{7/2}$ (138.13 eV), which reveal that the Pb primarily existed in bivalent [40–42] in the $Pb_{0.04}$Co(CP) catalyst, though Pb_3O_4 phase together with PbO was detected by XRD on the PbO_x (CP) sample.

Maniak et al. [36] found that K^+ cations primarily weakens the Co—O bond of octahedral Co^{3+} in the cobalt spinel, leading to reducibility of the Co^{3+} increasing, and that the spinel doped with K_2CO_3 was more active for the reaction and easier to be reduced than those doped with other potassium precursors. Therefore authors proposed that the octahedral Co^{3+} cations are active sites for catalyzing the reaction. Actually, the active sites is changed in cycle between Co^{3+} and its lower valence, which was widely known as cationic redox mechanism [14,18,24,29]. As the active state of the active sites, which leads to N_2O molecules decomposing to N_2 and O_{ad}, it must be capable to receive the oxygen resulted from N_2O decomposition. It means that the active state of the active sites must possess one oxygen vacancy. Thus, the change of the octahedral cobalt cations in valence and in oxygen coordination along with catalytic cycles can be represented in Fig. 4, according to the redox reaction mechanism [36,43].

The oxygen vacancy on the catalyst surface was measured by O_2 pulse adsorption (Fig. 5). By pretreating the catalyst sample (in He 300 °C for 20 min), the O atoms adsorbed on the catalyst surface and the O^{2-} ions weakly bonded to Co^{2+} cations will escape from the catalyst surface, forming oxygen vacancies over there. The latter will be detected by the subsequent O_2 pulse adsorption at appropriate temperature. Hence, by integrating each response area with respect to that being reached to saturated adsorption over the catalysts, the amount of O_2 adsorbed on the oxygen vacancies can be estimated. They were 5.27 μmol g^{-1} for $Pb_{0.04}$Co(CP), and 2.55 μmol g^{-1} for Co_3O_4(CP). As the catalysts were pretreated at 300 °C in situ and the O_2 adsorption was conducted at 100 °C, the oxygen vacancies produced on each catalyst should be at least larger than twice of them.

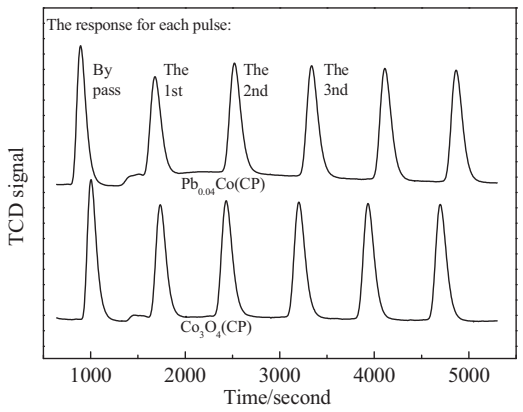

Fig. 5. Pulse adsorption of O_2 on the catalyst samples* at 100 °C.
**Note*: The samples had been activated in situ at 300 °C in He for 20 min before the experiment.

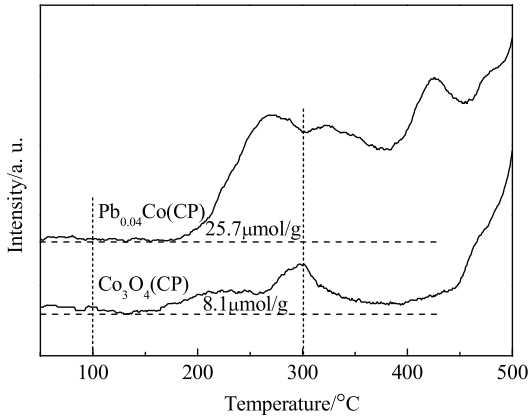

Fig. 6. O_2-TPD profiles of the catalyst samples* in He.
**Note*: Saturated adsorption of O_2 on the samples had been done in situ at 100 °C before the experiment.

O_2-TPD on the catalysts represented the similar results. As shown in Fig. 6, $Pb_{0.04}$Co(CP) gave much larger O_2 desorption area in the temperature range of 100–300 °C compared with Co_3O_4(CP). Accordingly, the accumulation O_2 amount over $Pb_{0.04}$Co(CP) and Co_3O_4(CP) were 25.7 and 8.1 μmol g^{-1}, respectively. For the two catalysts, by combining the O_2 desorption amounts with their BET surface areas (in Table 1), their oxygen vacancy densities were further calculated. It was 0.40 μmol m^{-2} for $Pb_{0.04}$Co(CP) and 0.69 μmol m^{-2} for Co_3O_4(CP). Clearly, if one presumes that the oxygen vacancy is exclusively produced at Co_3O_4 surface, the results will also strongly support our conclusion that Pb predominantly present at the $Pb_{0.04}$Co(CP) catalyst surface. The reason is that the Co_3O_4 surface is covered by Pb to some extent in this case, though the Pb content in the catalyst was rather little.

3.2. Catalytic performance of the Pb_{04}Co(CP) catalysts

3.2.1. For the feed gas of 2000 ppmv N_2O/Ar

The catalytic performance of the Pb_xCo(CP) catalysts with Pb/Co molar ratio x in the range of 0–0.1 in the reaction is shown in Fig. 7. Compared with Co_3O_4(CP), all the Pb_xCo(CP) catalysts displayed higher activity for the reaction. For the Pb_xCo(CP) catalysts,

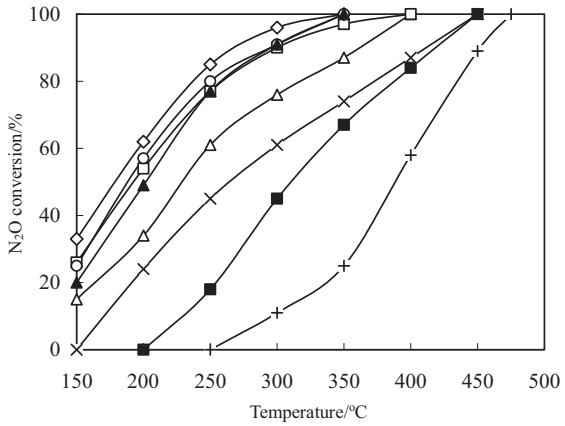

Fig. 7. N_2O conversion over the Pb_xCo(CP) catalysts (x = 0 (+), 0.01 (×), 0.02 (Δ), 0.03 (□), 0.04 (◊), 0.05 (○), 0.06 (▲), 0.1 (■)) for feed gas 2000 ppmv N_2O/Ar.

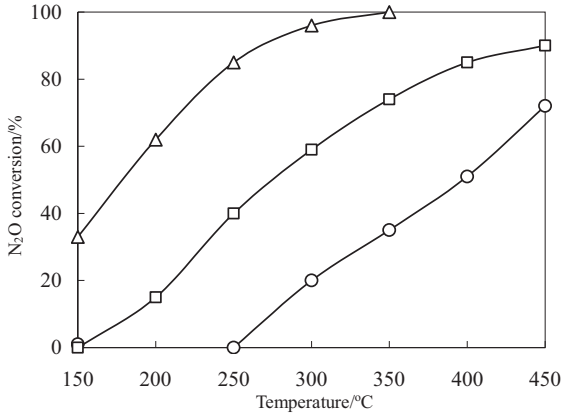

Fig. 8. N_2O conversion over $Pb_{0.04}Co$(CP) (Δ), $Pb_{0.04}Co$(IM) (□) and Co_3O_4(CP) (○) for feed gas 2000 ppmv N_2O/Ar.

interestingly, their optimal Pb/Co molar ratio appeared at 0.04, the such small ratio should be derived from their special structure: Pb predominantly presents on the Co_3O_4 crystallites' surface in the catalyst.

3.2.2. The mechanism of Pb improving the reaction

The N_2O decomposition taking place over the $Pb_{0.04}Co$(CP) and Co_3O_4(CP) catalyst in first order was confirmed both by our differential and integral reaction experiments. On the basis, the rate constants (k) at some definite temperatures and the active energy (E_a) of the reaction over $Pb_{0.04}Co$(CP) and Co_3O_4(CP) were detected in the feed gas of 2000 ppmv N_2O/Ar. Table 3 shows that the k at 300 °C were 1.56×10^{-5} $m^3\,s^{-1}\,g^{-1}$ for $Pb_{0.04}Co$(CP) and 6.54×10^{-7} $m^3\,s^{-1}\,g^{-1}$ for Co_3O_4(CP). Clearly, the much larger rate constants for $Pb_{0.04}Co$(CP) compared with Co_3O_4(CP), which was 24 times as high as that of the latter, should be derived from its larger amount of active sites and its possible larger turn over frequency (TOF) of the reaction at the active sites, in comparison with those of Co_3O_4(CP). Furthermore, the k at each reaction temperature and E_a were also estimated from our integral reaction data by calibrating the N_2O concentration change in the catalyst bed, as shown in the table. Quite closed data were obtained from the two methods.

For the catalytic N_2O decomposition, it was considered to be initiated by the step (I) over transitional metal oxides, i.e., N_2O reacting with the oxygen vacancies (*) that associated with the active sites [6,13,24,38],

$$N_2O + * \xrightarrow{k_1} N_2 + O - * \quad \text{(I)}$$

and the reaction is controlled by the oxygen desorption from the active sites occupied by oxygen in the step (2) [44].

$$2O - * \xrightarrow{k_2} O_2 + 2* \quad \text{(II)}$$

As described in Section 3.1, the $Pb_{0.04}Co$(CP) and Co_3O_4(CP) catalyst desorbed 25.7 and 8.1 μmol g^{-1} O_2 at the temperature below 300 °C in O_2-TPD, respectively, after a saturated O_2 desorption at 100 °C. Clearly, the results indicate the population of oxygen vacancies (51.4 μmol g^{-1} for $Pb_{0.04}Co$(CP) and 16.2 μmol g^{-1} for Co_3O_4(CP) that can be reproduced at 300 °C by the step (II), as just these part of oxygen vacancies can be expected to work on for catalyzing the reaction in the cycles (Fig. 4). On this basis, TOF of the reaction over the catalysts was calculated (Table 3), which indicates that the reaction occurs with 23.1×10^{-3} s^{-1} over $Pb_{0.04}Co$(CP) at 300 °C, with 3.1×10^{-3} s^{-1} over Co_3O_4(CP). Clearly, both the much larger TOF and the much lower E_a (28.9 kJ mol^{-1}) of $Pb_{0.04}Co$(CP) compared with those of Co_3O_4(CP) must be derived from the function of Pb weakening Co—O bond.

This property of Pb in $Pb_{0.04}Co$(CP) weakening the Co—O bond exerted its more significance when the reaction toke place over the catalyst in the feed gas with 5 vol% O_2 presence. As shown in Table 3, due to the introduction of 5 vol% O_2 into the feed gas, the k over Co_3O_4(CP) at 300 °C seriously decreased (from 6.54×10^{-7} to 1.55×10^{-7} $m^3\,s^{-1}\,g^{-1}$), which may be associated with the possible competitive adsorption of O_2 with N_2O on the oxygen vacancy. However, in the case of $Pb_{0.04}Co$(CP) catalyst, the k decreasing (from 1.56×10^{-5} to 1.15×10^{-5} $m^3\,s^{-1}\,g^{-1}$) caused by 5 vol% O_2 was quite limited. Clearly, this phenomena can be attributed to Pb weakening the Co—O bond and hence promotes the step (II), making the reaction over the catalyst hardly influenced by O_2.

Actually, the deduction that Pb in the $Pb_{0.04}Co$ catalyst plays the role of weakening Co—O bond and therefore increases the TOF of the reaction was verified by the reaction over $Pb_{0.04}Co$(IM). Since the catalyst was prepared by impregnating $Pb(NO_3)_2$ on the Co_3O_4(CP), it can be speculated that the $Pb_{0.04}Co$(IM) catalyst must have less active sites in population for catalyzing the reaction, as the Pb^{2+} cations could only presents the Co_3O_4 crystallite surface, and therefore block some active sites on the Co_3O_4 crystallite surface. However, as shown in Fig. 8, considerable higher N_2O conversion was obtained over $Pb_{0.04}Co$(IM) than that over Co_3O_4(CP).

Certainly, the $Pb_{0.04}Co$(IM) is not comparable with $Pb_{0.04}Co$(CP) in activity, due to the much more active sites of the latter in population, being derived from the special coprecipitation method for catalyst preparation.

3.2.3. For the feed gas of 2000 ppmv N_2O/Ar containing some impurities

Fig. 9 shows the N_2O reaction results over the $Pb_{0.04}Co$(CP) catalyst for the feed gas of 2000 ppmv N_2O together with 5 vol% O_2, 2 vol% H_2O, 500 ppmv NO, 10 vol% CO_2, or 50 ppmv SO_2 in Ar. The inhibition effect of the impurity gases on the reaction over the catalyst was quite limited. Over the catalyst, T_{90} (the temperature for N_2O conversion reaching 90%) of the reaction in the feed gas of 2000 ppmv N_2O/Ar was 270 °C. When 5 vol% O_2, 500 ppmv NO, 50 ppmv SO_2, 10 vol% CO_2, and 2 vol% H_2O was introduced into the feed gas, it increased to 309, 333, 305, 325 and 360 °C, respectively. Recently, it was reported that the T_{90} for the reaction of 1000 ppmv N_2O/N_2 over 0.01K-$Cu_{0.25}Co_{2.75}O_4$ catalyst from 310 °C increased to 350, 410, and 340 °C, respectively, due to 2 vol% O_2, 200 ppmv NO, or 0.5 vol% H_2O being introduced into the gas mixture [24]. Compared with the catalyst reported in literature, the $Pb_{0.04}Co$(CP) catalyst seems to be better on resisting the impurity gases.

As shown in Fig. 10, introduction of 10 vol% CO_2 together with 5 vol% O_2 into the feed gas just made the T_{90} increased to 336 °C. Clearly, the increment (66 °C) of T_{90} due to the presence of 10 vol%

Table 3
Active sites of the catalysts and kinetic parameters of the reaction over the catalysts.

Cat.	T (°C)	k($m^3\ s^{-1}\ g^{-1}$)[a]	k($m^3\ s^{-1}\ g^{-1}$)[b]	E_a (kJ mol^{-1})[a]	E_a (kJ mol^{-1})[b]	Active sites (μmol g^{-1})[c]	TOF (s^{-1})[d]
Co_3O_4	300	4.83×10^{-7}	6.54×10^{-7} 1.55×10^{-7} (O_2)	63.9	74.0	16.2 (5.1)	3.1×10^{-3}
	350	1.19×10^{-6}	1.77×10^{-6}				
	400	3.60×10^{-6}	6.64×10^{-6}				
$Pb_{0.04}Co$	200	4.23×10^{-6}	4.35×10^{-6}	25.9	28.9		
	250	7.87×10^{-6}	9.30×10^{-6}				
	300	1.33×10^{-5} 9.76×10^{-6} (O_2)	1.56×10^{-5} 1.15×10^{-5} (O_2)			51.4 (10.5)	23.1×10^{-3}

[a] Evaluated from integral reaction of 2000 ppmv N_2O + Ar with or without O_2 (5 vol%).
[b] Measured by differential reaction of 2000 ppmv N_2O + Ar.
[c] The data at 300 °C detected by O_2-TRD, while those in parentheses are detected by O_2 pulse adsorption.
[d] Calculated based on the data detected by differential reaction and O_2-TRD.

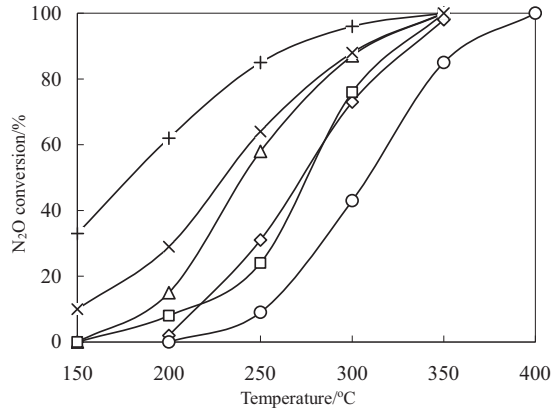

Fig. 9. N_2O conversion over the $Pb_{0.04}Co$(CP) catalyst for the feed gas 2000 ppmv N_2O/Ar(+); with 50 ppmv SO_2 (×), 5 vol% O_2 (Δ), 10 vol% CO_2 (□) 500 ppmv NO (◊), 2 vol% H_2O (○).

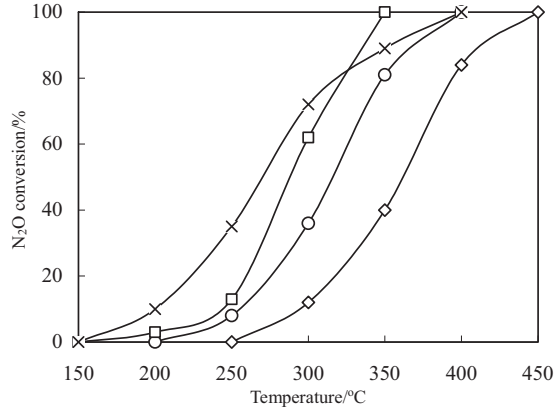

Fig. 10. N_2O conversion over the $Pb_{0.04}Co$(CP) catalyst for the feed gas 2000 ppmv N_2O with 10 vol% CO_2 + 5 vol% O_2 (□), 50 ppmv SO_2 + 5 vol% O_2 (×), 2 vol% H_2O + 5 vol% O_2 (○), or 500 ppmv NO + 5 vol% O_2(◊).

CO_2 + 5 vol% O_2 in the feed gas was much less than the sum of that caused by 10 vol% CO_2 (55 °C) and 5 vol% O_2 (39 °C) alone. Similarly, the increment of T_{90} (100 °C) caused by 5 vol% O_2 together with 2 vol% H_2O was less than the sum caused by the corresponding individual impurity gases. However, for 500 ppmv NO coexisting with 5 vol% O_2, and 50 ppmv SO_2 coexisting with 5 vol% O_2 in the feed gas, the increments were obviously larger than the corresponding sum. For instance, in the case of 500 ppmv NO + 5 vol% O_2, the N_2O conversion decreased from 100% to 40%, and in the case of 50 ppmv SO_2 + 5 vol% O_2, the N_2O conversion decreased from 100% to 89%. These phenomena may be associated with the possible formation

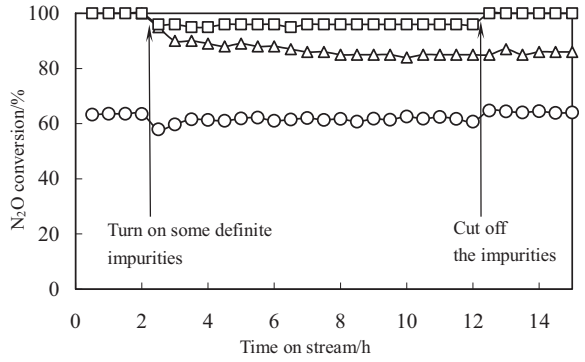

Fig. 11. N_2O conversion over $Pb_{0.04}Co$(CP) catalyst at 350 °C.
(Δ) Feeding gas 2000 ppmv of N_2O/Ar with or without 50 ppmv SO_2 + 5 vol% O_2 at 20000 h^{-1}; (○) Feeding gas 2000 ppmv of N_2O/Ar with or without 10 vol% CO_2 + 5 vol% O_2 at 20000 h^{-1}; (□) Feeding gas 2000 ppmv of N_2O/Ar + 100 ppmv NO + 5 vol% O_2 with or without 2 vol% H_2O at 10000 h^{-1}.

of NO_2 and SO_3 in gas phase as well as the formation of NO_2^-/NO_3^- and SO_4^{2-} on catalyst surface, which will be discussed later.

Table 4 summarized the transitional metal oxide based catalysts and zeolite based catalysts reported in literature concerning impurity gases. It can be found that the $Pb_{0.04}Co$(CP) catalyst reached to the same level in activity and in the resistance to general impurity gases. Furthermore, a large development was acquired for the $Pb_{0.04}Co$(CP) catalyst on the catalytic activity in the presence of CO_2, compared with our previously reported $Bi_{0.02}Co$ catalyst. For instance, the T_{90} in the presence of 5 vol% O_2 and 10 vol% CO_2 over $Bi_{0.02}Co$ was 405 °C, while over the $Pb_{0.04}Co$(CP) was 336 °C under the same reaction conditions.

3.2.4. Catalytic stability of the catalyst

The catalytic stability of the $Pb_{0.04}Co$(CP) catalyst was investigated under the conditions of 5 vol% O_2 + 10 vol% CO_2, 100 ppmv NO + 5 vol% O_2 + 2 vol% H_2O, or 50 ppmv SO_2 + 5 vol% O_2 existing in the feed gas.

As shown in Fig. 11, the influence of 5 vol% O_2 and 10 vol% CO_2 in the feed gas on the catalytic activity was rather little. Due to the impurity gases introduction, the N_2O conversion at 350 °C just decreased to 96% from the original 100%. Moreover, the activity of the catalyst was much stable under the O_2 and CO_2 coexisting conditions. It can be known from the following phenomena: (1) The N_2O conversion over the catalyst did not further decline from the initial value (96%) under the impurity gases existing conditions with time on stream; (2) The conversion over the catalyst instantly recovered upon the impurity gases being cut off from the feed gas. Obviously, the influence of CO_2 and O_2 on the reaction only results from dynamics.

The $Pb_{0.04}Co$(CP) catalyst displayed quite stable catalytic performance as well in the feed gas 2000 ppmv of N_2O/Ar + 100 ppmv

Table 4
Comparison of the $Pb_{0.04}Co$ catalyst with those recently reported in literature on the activity for N_2O decomposition in presence of impurity gases.

Catalysts	Feed gas and GHSV (or *W*/*F*) of the reaction	T_{90}[a]	Pub. year	Refs.
ex-	1500 ppmv N_2O and 333 ppmv NO; 60000 h^{-1}	402	2002	[12]
FeZSM-	1500 ppmv N_2O and 0.5 vol% CO_2; 60000 h^{-1}	502		
5	1500 ppmv N_2O and 250 ppmv SO_2; 60000 h^{-1}	477		
FeRu-FER-2	1500 ppmv N_2O and 400 ppmv NO; 60000 h^{-1}	420	2006	[25]
$CoCe_{0.05}$	1000 ppmv N_2O and 500 ppmv NO; 15000 h^{-1}	380	2007	[20]
Fe(III)-USY	1500 ppmv N_2O and 200 ppmv NO; 30000 h^{-1}	430	2008	[26]
CoMOR130-BIE	5000 ppmv N_2O and 1000 ppmv NO; 30000 h^{-1}	410	2011	[28]
1 wt% $Ag/La_{0.8}Ba_{0.2}MnO_3$	5000 ppmv N_2O, 0.02 vol% NO and 5 vol% O_2; 7500 h^{-1}	480	2011	[29]
CoFe-MOR	5000 ppmv N_2O and 1000 ppmv NO; 30000 h^{-1}	410	2012	[30]
$Rh/CeO_2(Pr)/-Al_2O_3$	1000 ppmv N_2O, 2 vol% O_2, and 1000 ppmv NO; 30000 h^{-1}	450	2012	[31]
3 wt.% Co/Beta	0.5 vol% N_2O, 600 ppmv NO and 5 vol% O_2; 30000 h^{-1}	435	2012	[32]
Fe-Beta/meso	5000 ppmv N_2O and 200 ppmv NO; 0.12 g s cm^{-3}	440	2015	[22]
$10\text{-}Cu/CeO_2\text{-}160$	2500 ppmv N_2O and 1.5 vol.% NO; 45000 h^{-1}	500	2015	[33]
CoIn-MOR	5000 ppmv N_2O, 1000 ppmv NO; 30000 h^{-1}	440	2015	[23]
$0.01K\text{-}Cu_{0.25}Co_{2.75}O_4$	1000 ppmv N_2O and 200 ppmv NO; 54000 h^{-1}	405	2015	[24]
$Bi_{0.02}Co$	2000 ppmv N_2O, 5 vol% O_2 and 10 vol% CO_2; 20000 h^{-1}	405	2015	[34]
$K_{0.01}Co$	2000 ppmv N_2O and 10 vol% CO_2; 20000 h^{-1}	390	2015	[34]
$Pb_{0.04}Co$	2000 ppmv N_2O, 5 vol% O_2 and 500 ppmv NO; 20000 h^{-1}	414	–	Thiswork
	2000 ppmv N_2O, 5 vol% O_2 and 50 ppmv SO_2; 20000 h^{-1}	354		
	2000 ppmv N_2O, 5 vol% O_2 and 10 vol% CO_2; 20000 h^{-1}	336		

[a] *Note*: The reaction temperature (°C) for 90% N_2O conversion over the corresponding catalysts.

NO + 5 vol% O_2 + 2 vol% H_2O during the reaction time on stream of 15 h at 350 °C. For the catalyst, although its initial activity in this case was much lower than that of no impurities existing in feed gas, the activity did not further decline with time on stream, despite of H_2O presence or absence. It means that the activity suppression due to the impurities is also just caused by dynamic reason.

When 50 ppmv SO_2 + 5 vol% O_2 was introduced into the feed gas as impurities, the case was quite different. The catalyst activity did not recover after the impurities were cut off. It was reported that SO_4^{2-} rapidly deposits on Co_3O_4 spinel catalyst when the catalyst was exposed to $SO_2 + O_2$ gas mixture [45]. Nevertheless, the activity declining caused by 50 ppmv SO_2 + 5 vol% O_2 seems to be not much severe for the $Pb_{0.04}Co$(CP) catalyst. The N_2O conversion finally maintained at ~85% after the reaction conducted for 10 h with time on stream at 350 °C.

4. Conclusions

By doping Co_3O_4 with Pb, a highly active $Pb_{0.04}Co$(CP) catalyst for N_2O decomposition was prepared. In this catalyst, the Co_3O_4 existed as crystallites with the diameter about 12 nm, which was significantly associated with the additive Pb and coprecipitation method for preparing the catalyst. As the radius of Pb^{2+} is too large to be accepted by the Co_3O_4 crystal lattice, Pb^{2+} played a role of decreasing the average size of the Co_3O_4 crystallites in the $Pb_{0.04}Co$(CP) catalyst. Due to this reason, the surface area and active sites in population for the $Pb_{0.04}Co$(CP) catalyst catalyzing the reaction was greatly increased.

Another function of Pb in the $Pb_{0.04}Co$(CP) catalyst was weakening the Co—O bond, which was strongly supported by the band shifting with respect to that of Co_3O_4(CP) in the CO adsorption IR spectra. It was also supported by the kinetic parameters, such as the *k*, E_a, as well as TOF, of the reaction over the two catalysts obtained from dynamic study. Over Co_3O_4(CP), the E_a for the reaction was 74.0 kJ mol^{-1}, while over $Pb_{0.04}Co$(CP), it was lowered to 28.9 kJ mol^{-1}. Correspondingly, the TOF over $Pb_{0.04}Co$(CP) at 300 °C was 23.1×10^{-3} s^{-1}, which was about seven times as high as that over Co_3O_4(CP) (3.1×10^{-3} s^{-1}) at the same reaction temperature.

The N_2O decomposition over the $Pb_{0.04}Co$(CP) catalyst in the presence of 5 vol% O_2, 2 vol% H_2O, 500 ppmv NO, 10 vol% CO_2, 50 ppmv SO_2, and some of them was investigated. The largest impact was caused from the NO together O_2, which led to a suppression of the N_2O conversion from 100% to 40% at 350 °C. CO_2 had almost no influence on the reaction over the $Pb_{0.04}Co$(CP) catalyst, which may allow the catalyst eliminating N_2O from the exhausts containing CO_2 in large concentration. The $Pb_{0.04}Co$(CP) catalyst displayed quite stable catalytic performance in the feed gas 2000 ppmv of N_2O/Ar + 100 ppmv NO + 5 vol% O_2 + 2 vol% H_2O during the reaction time on stream of 15 h at 350 °C.

Acknowledgment

This work was financially supported by the National Natural Science Foundation of China (Grant Nos. 21177016 and 21277019).

Appendix A. Supplementary data

Supplementary data associated with this article can be found, in the online version, at http://dx.doi.org/10.1016/j.apcatb.2015.12.011.

References

[1] R.E. Dickinson, R.J. Cicerone, Nature 319 (1986) 109–115.
[2] J. Pérez-Ramırez, F. Kapteijn, K. Schöffel, et al., Appl. Catal. B 44 (2003) 117–151.
[3] N. Liu, R.D. Zhang, B.H. Chen, Y.P. Li, Y.X. Li, J. Catal. 294 (2012) 99–112.
[4] V.G. Komvokis, G.E. Marnellos, I.A. Vasalos, K.S. Triantafyllidis, Appl. Catal. B 89 (2009) 627–634.
[5] J. Pérez-Ramírez, Appl. Catal. B 70 (2007) 31–35.
[6] F. Kapteijn, J. Rodriguez-Mirasol, J.A. Moulijn, Appl. Catal. B 9 (1996) 25–64.
[7] B.M. Abu-Zied, S.A. Soliman, S.E. Abdellah, Chin. J. Catal. 35 (2014) 1105–1112.
[8] J.N. Armor, T.A. Braymer, T.S. Farris, Y. Li, F.P. Petrocelli, E.L. Weist, S. Kannan, C.S. Swamy, Appl. Catal. B 7 (1996) 397–406.
[9] R.A. Reimer, C.S. Slaten, M. Seapan, M.W. Lower, P.E. Tomlinson, Environ. Prog. 13 (1994) 134–137.
[10] B.W. Riley, J.R. Richmond, Catal. Today 17 (1993) 277–284.
[11] J.N. Armor, T.S. Farris, Appl. Catal. B 4 (1994) 11–17.
[12] J. Pérez-Ramírez, F. Kapteijn, G. Mul, X.D. Xu, J.A. Moulijn, Catal. Today 76 (2002) 55–74.
[13] N. Russo, D. Fino, G. Saracco, V. Specchia, Catal. Today 119 (2007) 228–232.
[14] K. Asano, C. Ohnishi, S. Iwamoto, Y. Shioya, M. Inoue, Appl. Catal. B 78 (2008) 242–249.
[15] N. Pasha, N. Lingaiah, N.S. Babu, P.S. Sankar Reddy, P.S. Sai Prasad, Catal. Commun. 10 (2008) 132–136.
[16] N. Pasha, N. Lingaiah, P.S.S. Reddy, P.S.S. Prasad, Catal. Lett. 127 (2009) 101–106.
[17] L. Yan, T. Ren, X.L. Wang, D. Ji, J.S. Suo, Appl. Catal. B 45 (2003) 85–90.
[18] P. Stelmachowski, G. Maniak, A. Kotarba, Z. Sojka, Catal. Commun. 10 (2009) 1062–1065.
[19] N. Pasha, N. Lingaiah, P. Siva Sankar Reddy, P.S. Sai Prasad, Catal. Today 118 (2007) 64–68.
[20] L. Xue, C.B. Zhang, H. He, Y. Teraoka, Appl. Catal. B 75 (2007) 167–174.

[21] L. Kuboňová, D. Fridrichová, A. Wach, P. Kustrowski, L. Obalová, P. Cool, Catal. Today 257 (2015) 51–58.
[22] M. Rutkowska, Z. Piwowarska, E. Micek, L. Chmielarz, Microporous Mesoporous Mater. 209 (2015) 54–65.
[23] X.Y. Zhang, Y.Y. Guan, S.Q. Zhang, M. Yang, Y. Zhao, Z.P. Hao, J. Mol. Catal. A: Chem. 395 (2014) 202–209.
[24] T. Franken, R. Palkovits, Appl. Catal. B 176–177 (2015) 298–305.
[25] G.D. Pirngruber, L. Frunz, J.A.Z. Pieterse, J. Catal. 243 (2006) 340–349.
[26] L.D. Li, Q. Shen, J.J. Li, Z.P. Hao, Z.P. Xu, G.Q. Max Lu, Appl. Catal. A 344 (2008) 131–141.
[27] Q. Shen, L.D. Li, J.J. Li, H. Tian, Z.P. Hao, J. Heterocycl. Chem. 163 (2009) 1332–1337.
[28] X.Y. Zhang, Q. Shen, C. He, Y.F. Wang, J. Cheng, Z.P. Hao, J. Hazard. Mater. 192 (2011) 1756–1765.
[29] S. Kumar, Y. Teraoka, A.G. Joshi, S. Rayalu, N. Labhsetwar, J. Mol. Catal. A-Chem. 348 (2011) 42–54.
[30] X.Y. Zhang, Q. Shen, C. He, C.Y. Ma, J. Cheng, Z.P. Hao, Catal. Sci. Technol. 2 (2012) 1059–1067.
[31] S. Parres-Esclapez, M.J. Illán-Gómez, C. Salinas-Martínez de Lecea, A. Bueno-López, Int. J. Greenh. Gas Control 11 (2012) 251–261.
[32] Q. Shen, L.D. Li, C. He, X.Y. Zhang, Z.P. Hao, Z.P. Xu, J. Chem. Eng. 7 (2012) 502–509.
[33] M. Zabilskiy, P. Djinovic, B. Erjavec, G. Drazic, A. Pintar, Appl. Catal. B 163 (2015) 113–122.
[34] M. Tursun, X.P. Wang, F.F. Zhang, H.B. Yu, Catal. Commun. 65 (2015) 1–5.
[35] L. Río, G. Marbán, Appl. Catal. B 126 (2012) 39–46.
[36] G. Maniak, P. Stelmachowski, A. Kotarba, Z. Sojka, V. Rico-Pérez, A. Bueno-López, Appl. Catal. B 136–137 (2013) 302–307.
[37] H.K. Cheng, Y.Q. Huang, A.Q. Wang, L. Li, X.D. Wang, T. Zhang, Appl. Catal. B 89 (2009) 391–397.
[38] J.L. Zhang, H. Hu, J. Xu, G.M. Wu, Z.W. Zeng, J. Environ. Sci. 26 (2014) 1437–1443.
[39] Y. Okamoto, H. Nakano, T. Imanaka, S. Teranishi, Bull. Chem. Soc. Jpn. 48 (1975) 1163–1168.
[40] J.M. Thomas, M.J. Tricker, J. Chem. Soc. Faraday Trans. II 71 (1975) 329–336.
[41] A. Hrussanova, L. Mirkova, T. Dobrev, J. Appl. ElectroChem. 32 (2002) 505–512.
[42] N. Kannadasan, N. Shanmugam, K. Sathishkumar, S. Cholan, R. Ponnguzhali, G. Viruthagiri, SpectroChim. Acta A 143 (2015) 179–186.
[43] P. Pietrzyk, F. Zasada, W. Piskorz, A. Kotarba, Z. Sojka, Catal. Today 119 (2007) 219–227.
[44] L. Obalová, K. Jirátová, F. Kovanda, M. Valášková, J. Balabánová, K. Pacultová, J. Mol. Catal. A 248 (2006) 210–219.
[45] X.Y. Shi, Y.B. Yu, L. Xue, H. He, Chin. J. Catal. 35 (2014) 1504–1510.